Terahertz radar cross section measurements

Krzysztof Iwaszczuk[a], Henning Heiselberg[b], Peter Uhd Jepsen[a]
[a] DTU Fotonik – Deparment of Photonics Engineering, Technical University of Denmark, DK-2800 Kgs. Lyngby, Denmark
[b] Danish Defense Acquisition & Logistics Organization, DK – 2750 Ballerup, Denmark

***Abstract*—We present the result of terahertz radar cross section measurements on various objects including models of aircraft fighters. Application of a time domain system provides both values of radar cross section and ranging information.**

I. Introduction And Background

Scattering of terahertz (THz) waves by conducting and dielectric objects is an area of intensive investigation both on ground of theory and experiment [1-5]. Radar cross section (RCS) measurements are particularly important for military and defense-related purposes, including detection of aircrafts, ships and other targets as well as for counter measures such as RCS reduction and stealth. Time domain based THz systems can provide a convenient, fast and precise method to measure multiband RCS of scale models in tabletop experiments, providing at the same time ranging information.

In this work we measure THz RCS of scale models and present polar and azimuthal angle and time resolved RCS plots of F-16 fighter aircraft model rotated on a pedestal. The time domain sub-ps resolution allows for sub-mm range resolution that can be found in modern software defined radars. The range, polar and azimuthal RCS plots are analogous to inverted synthetic aperture radar images (ISAR) in three dimensions [6-8]. The resulting RCS and ISAR images can be compared to measurements on real aircrafts, ships and other platforms by simple scaling.

II. Results

Figure 1(a) presents a schematic diagram of the terahertz radar cross section setup. ~35-fs, 3.1 mJ pulses with a central wavelength of 800 nm from a regenerative Ti:sapphire femtosecond laser amplifier is used to generate a THz radiation in a 1% MgO doped stoichiometric lithium niobate $LiNbO_3$ crystal by optical rectification with tilted pulse front method [9]. A pair of off-axis parabolic mirrors with focal lengths of 25.4 mm and 516.8 mm is used to expand and collimate the THz beam. Terahertz radiation traveles 120 cm before it reaches the computer-controlled rotation platform. The targets are placed on a polystyrene column, shaped such that all incoming THz radiation is reflected away from detector. Scattered radiation is collected at an angle of 6.6° with respect to the incoming THz light, focused by 6″ off-axis parabolic mirror and detected via free space electro-optic sampling in a stacked pair [110] – [100] of 2 mm-thick ZnTe crystals. The THz part of the setup is enclosed and purged with dry nitrogen to minimize water absorption lines. Figure 1(b) shows the amplitude of detected THz radiation. The amplitude extends from 0.02 THz up to 3 THz, but over 95% of the generated THz energy lies within 0.1 – 1.0 THz range. The setup was calibrated by substitution method using conducting spheres. The smallest detectable objects in our setup have RCS of 0.78 mm^2 with a FWHM of the THz beam of 73mm at the target position.

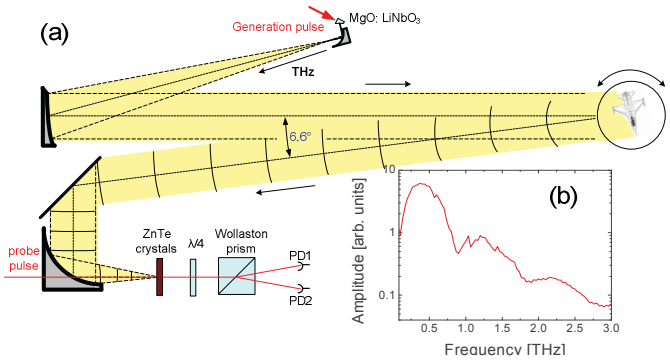

Fig. 1. (a) Schematic diagram of the THz radar cross section setup. (b) Amplitude spectrum of the generated terahertz radiation.

The radar cross section of a scattering object illuminated with radar radiation is a parameter expressed in units of area which describes the intensity of the wave reflected back to the radar [11 - 13]. In the ideal case, measured object should be illuminated with plane wave and scattered radiation should be collected at infinite distance from the target. For complex structures we can introduce the frequency-averaged radar cross section given by:

$$RCS = \pi a^2 \cdot \frac{\int_0^T \left|E_{object}(t)\right|^2 dt}{\int_0^T \left|E_{cal}(t)\right|^2 dt - \int_0^T \left|E_{bg}(t)\right|^2 dt},$$

where $E_{object}(t)$ is the detected electric from the scattering object, $E_{cal}(t)$ the electric field scattered by the calibrated spheres of radar cross section of πa^2, and the $E_{bg}(t)$ represents background noise. Since we measure not only the intensity of electromagnetic radiation but the field itself we can introduce the frequency resolved *RCS* defined as follows:

$$RCS(\omega) = \pi a^2 \cdot \frac{\left|E_{object}(\omega)\right|^2}{\left|E_{cal}(\omega)\right|^2 - \left|E_{bg}(\omega)\right|^2},$$

where $E_i(\omega)$ is the Fourier transform of $E_i(t)$.

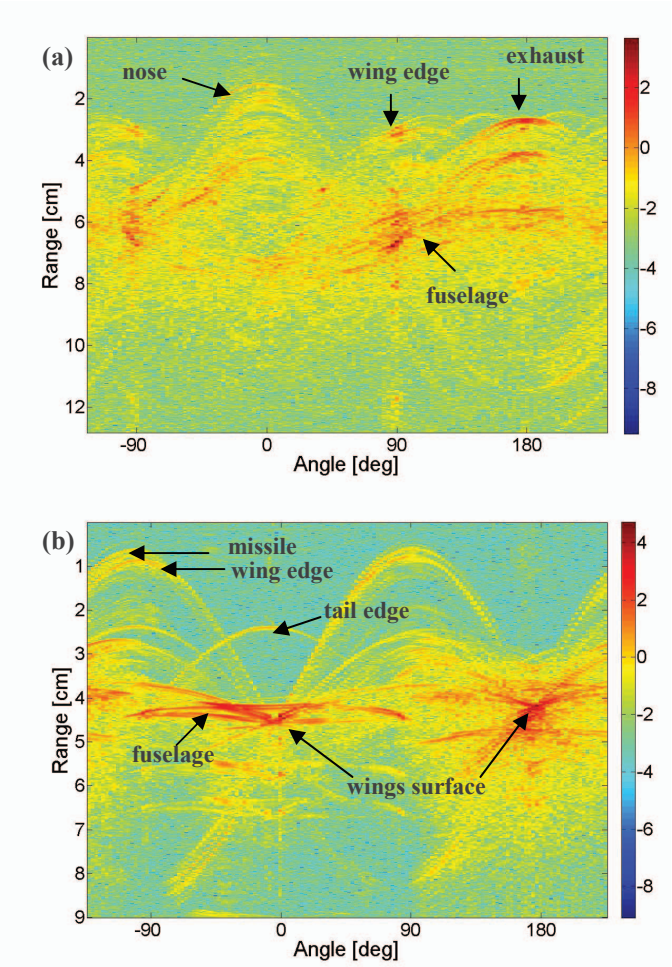

Fig. 2. Logarithm of absolute value of Hilbert transform of THz waveforms scattered from a 1:150-scale metal model of aircraft fighter F-16 vs. (a) polar and (b) azimuthal angle and range.

Figure 2 shows the logarithm of the absolute value of the Hilbert transform of the THz waveform vs. (a) polar and (b) azimuthal angle and range (calculated from the time delay and the speed of light), recorded for the metal 1:150-scale model of F-16 fighter. Single point scattering object is seen at those images as a sine function, therefore those maps are called sinograms. Before analyzing presented sinograms we have to point out that big flat surfaces give high THz reflection peaks in a very narrow angle range, while round shapes scatter light more uniformly. 0° position on Fig. 2(a) corresponds to position where the nose of airplane faces incoming THz radiation, while at 180° it is the exhaust pipe that is exposed to terahertz wave first. Careful analyzes of recorded waveforms on Fig. 2(a) indicates THz waves scattering from such parts of airplane as ends of wings, exhaust pipe, fuselage etc. On the azimuthal map orientation 0° corresponds to the situation at which airplane is exposed to THz radiation from above. THz reflections from various parts of model (wings, tail, fuselage, missiles, etc.) can be distinguished. Due to echoes in the THz waveforms, originating in pulse reflections in the generation and detection crystal, presented sinograms contain weak artifacts.

Figure 3 presents THz values of frequency-averaged RCS as a function of (a) polar and (b) azimuthal angle. For the polar configuration the smallest RCS is measured in a wide angle range in front of the airplane. The largest RCS is seen from the side of the model. The RCS plot is rotated counter-clockwise with respect to the orientation of the symmetry plane. The asymmetry of the plot can be explained as combination of 6.6° bistatic THz radar setup and possible small azimuthal tilt of the model. Analyzing Fig. 3(b) we can notice that the largest RCS in azimuthal configuration is for the airplane seen exactly from below and above. The smallest RCS is just below wings. The RCS plot is again counter-clockwise rotated with respect to the orientation of the symmetry plane, due to the bistatic nature of measurement.

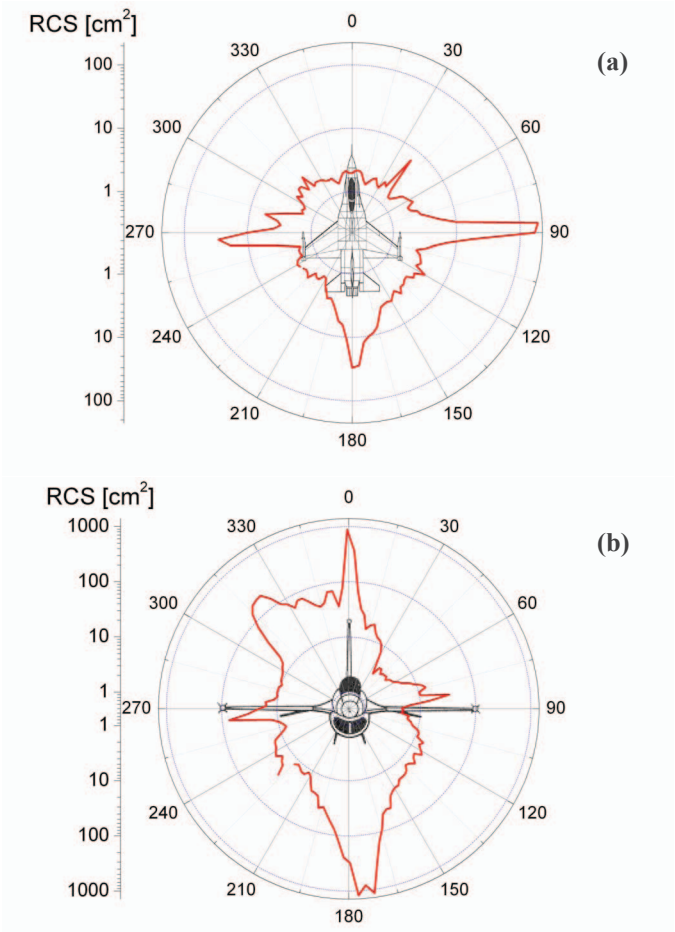

Fig 3. Frequency-averaged (a) polar and (b) azimuthal RCS of the model of aircraft fighter F-16.

Figure 4 presents values of frequency-resolved THz radar cross sections of scale model of F-16 fighter in the azimuthal configuration for frequencies 0.3, 0.7 and 1.1 THz. It can be noticed that at angles, where THz waves are reflected from big flat surfaces (0° and 180° - from the wing surfaces and at 90° and 270° from the tail surface), the RCS for high frequencies is larger than for low frequencies, what is in agreement with frequency dependent nature of wave scattering by objects with different curvature [11].

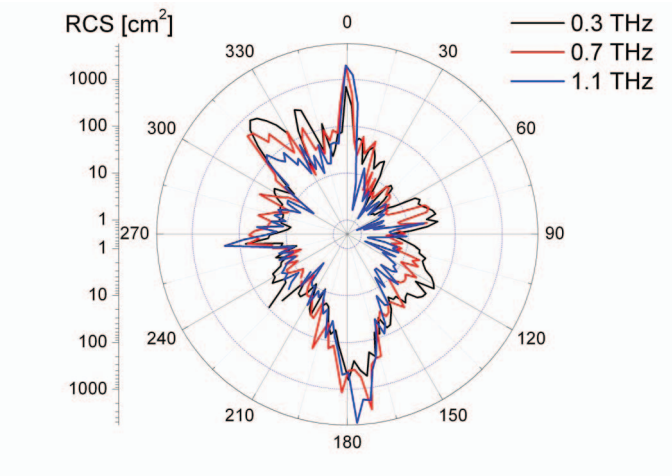

Fig 4. Frequency-resolved azimuthal RCS of a metal model of aircraft fighter F-16 for frequencies 0.3, 0.7 and 1.1 THz. Presented data are results of averaging within +/- 20GHz range.

III. CONCLUSSIONS

We have presented a method for bistatic radar cross section measurements using high-frequency THz waves. We have performed a series of RCS measurements of scale model of aircraft fighter F-16 both in the polar and azimuthal orientation. By scaling wavelengths and models to real-scale platforms we can accurately compare results to RCS at standard GHz and MHz frequencies. Our application of a time domain system allows not only for determination of *RCS* values but also for determination of *RCS* of particular elements of the model from sinograms in high range resolution maps vs. polar and azimuthal angles.

ACKNOWLEDGMENT

We are grateful to the Danish Defense Acquisition and Logistics Organization and Photonics Academy Denmark for financial support.

REFERENCES

[1] R. A. Cheville and D. Grischkowsky, "Time domain terahertz impulse ranging studies," Appl. Phys. Lett. **67**, 1960 (1995)
[2] R. A. Cheville, R. W. McGowan and D. R. Grischkowsky, "Late-time target response measured with terahertz impulse ranging," IEEE Trans. Antennas Propag. **45**, 1518 (1997)
[3] J. Pearce, D. M. Mittleman, "Using terahertz pulses to study light scattering," Phys. B **338**, 92 (2003)
[4] X. J. Zhong, T. J. Cui and Z. Li, "Terahertz-wave scattering by perfectly electrical conducting objects," J. Electromagn. Waves Appl. **21**, 2331 (2007)
[5] J. Pearce and D. M. Mittleman, "Scale model experimentation: using terahertz pulses to study light scattering," Phys. Med. Biol. **47**, 3823 (2002)
[6] J. Pearce, H. Choi, D. M. Mittleman, J. White and D. Zimdars, "Terahertz wide aperture reflection tomography," Opt. Lett. **30**, 1653 (2005)
[7] K. McClatchey, M. T. Reiten, and R.A. Cheville, "Time resolved synthetic aperture terahertz impulse imaging", Appl. Phys. Lett. **27**, 4485 (2001)
[8] T. M. Goyette, J. C. Dickinson, J. Waldman, W. E. Nixon, "A 1.56THz compact radar range for W-band imagery of scale-model tactical targets, " Proc. SPIE, Algorithms for Synthetic Aperture Radar Imagery VII, **4053**, 615 (2000)
[9] K.–L. Yeh, M. C. Hoffmann, J. Hebling and K. A. Nelson, "Generation of 10 μJ ultrashort terahertz pulses by optical rectification," App. Phys. Lett. **90**, 171121 (2007)
[10] E. F. Knott, "Radar cross section measurements," Van Nostrand Reinhold, New York, 1993
[11] D. L. Mensa, "High resolution radar cross-section imaging," Artech House, Boston, 1991
[12] N. J. Willis, "Bistatic Radar", 2nd Edition, Technology Service Corporation, 1995.